Report on experiment ES-386 performed at ID-18 on July 2016.

SMS results on Fe-partitioning between Ferropericlase and Bridgmanite

We recorded SMS spectra after the sample transformation of our glass starting material at high temperatures at pressures up to 141 GPa. According to the chemical composition of the ^{57}Fe-bearing starting material, we expect a mineral mixture composed of Bg, Fp and $CaSiO_3$ perovskite (CaPv). The complete sample transformation was monitored based on (i) our knowledge of the minimum time and temperature requested for the transformation [5] and (ii) the change with temperature and time of SMS features. For example, the main absorption peak of the compressed glass and the transformed sample (Fig. 1) plot around -0.5 mm/s or + 0.5 mm/s, respectively, at high pressures. At lower pressures, an intense contribution at 2-2.5 mm/s is present in the starting glass and not in the transformed sample.

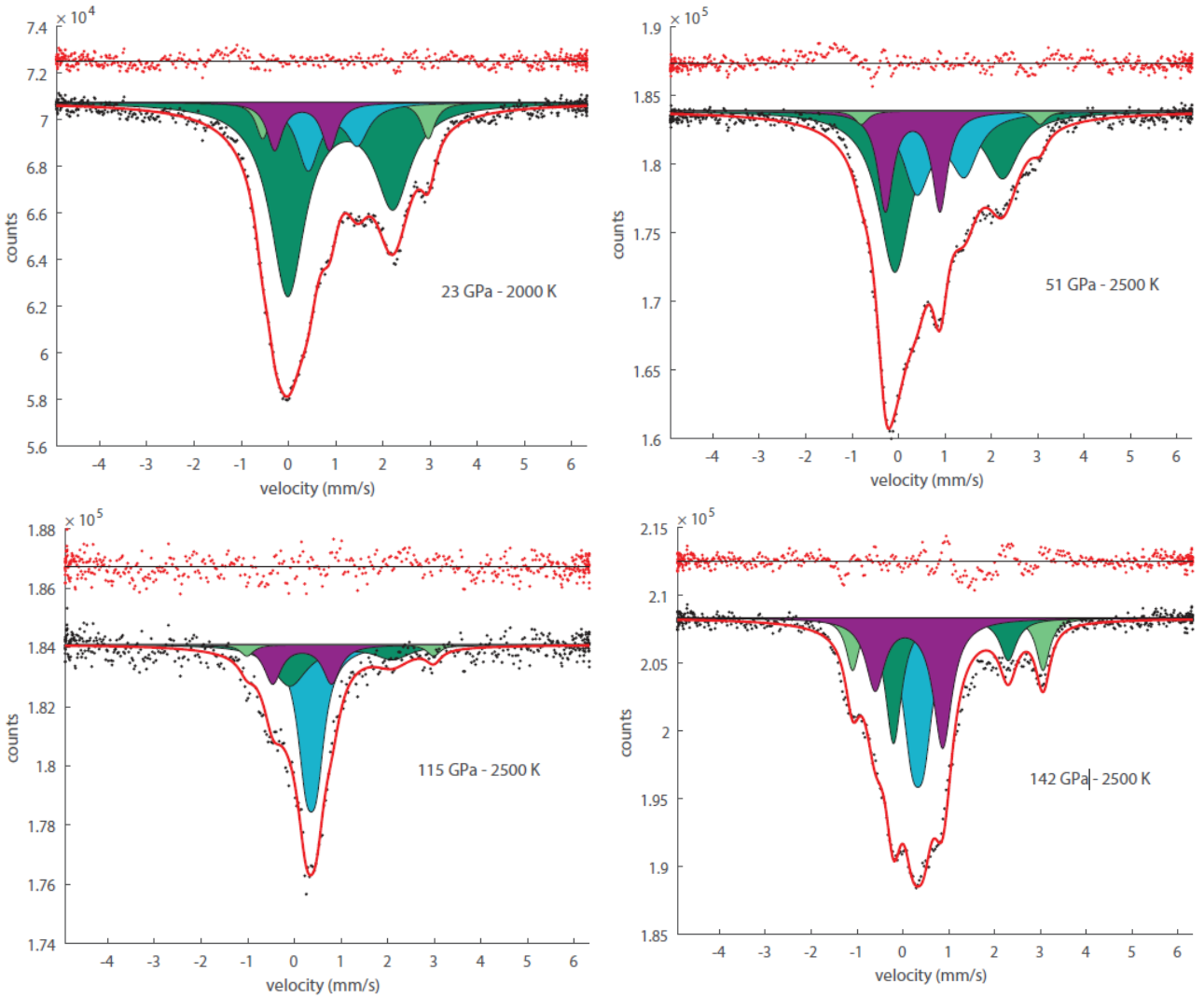

Figure 1: Typical fit of SMS patterns. Spectra were recorded at 300 K after synthesis at nominal pressures of 23 GPa (upper-left), 51 GPa (upper-right), 115 GPa (lower-left) and 142 GPa (lower-right). The five different contributions are high-spin Fe^{2+} and low-spin Fe^{2+} in Fp (Blue doublet and singlet, respectively), high-spin Fe^{2+} (Dark green doublet), intermediate-spin Fe^{2+} (Light green doublet) and high-spin Fe^{3+} (purple doublet) in Bg.

We used previous works to constrain the pressure evolution of CS and QS for Fe located in different atomic sites, with different ionic charges and different spin states. All our SMS patterns could be fitted by a sum of 5 different Fe contributions: high-spin Fe^{2+} and low-spin Fe^{2+} in Fp [8], high-spin Fe^{2+} with low-QS, intermediate-spin Fe^{2+} and high-spin Fe^{3+} in Bg [9,10] (Fig. 1). Due to a large number of parameters, we first adjusted the intensity of each band with all CS and QS values fixed to those reported in the literature. Then, we refined CS and QS to optimize the fit quality. All parameters remain at values compatible with previous works, within experimental uncertainties (Fig. 2a).

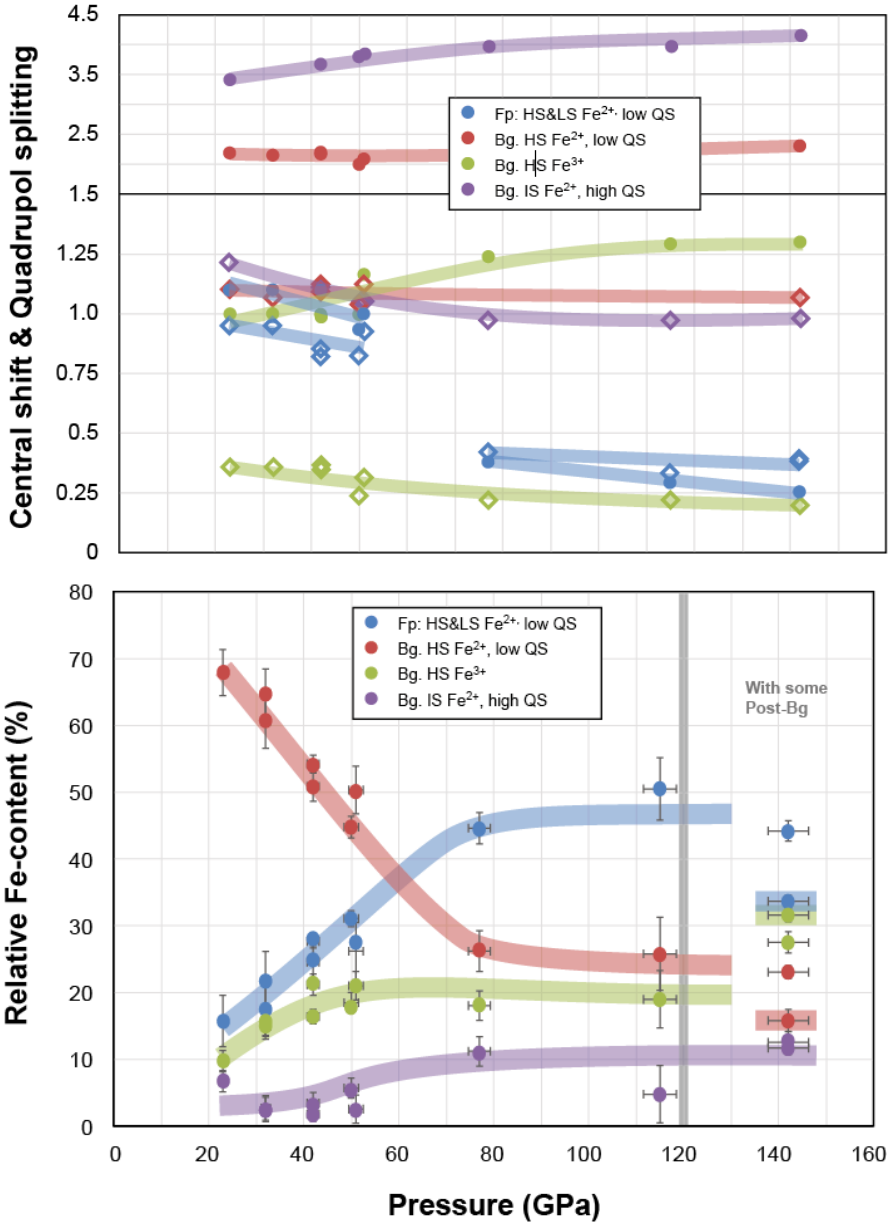

Figure 2: SMS results for transformed samples. (a) CS (open lozenges) and QS (circles) are reported for the 5 Fe contributions used to refined the SMS spectra: Two contributions for Fp are high-spin (low P) and low-spin (high P) Fe^{2+} (reported as a single contribution in blue); Three contributions for Bg are high-spin low-Q Fe^{2+} (red), high-spin Fe^{3+} (green) and intermediate-spin Fe^{2+} (purple). (b) Relative intensities refined for the different Fe-contributions. At 142 GPa, a major fraction of post-Bg is expected in the sample [5,6]. We performed two synthesis temperature of ~2500 K (with colored bars) and ~3500 K.

From the refined SMS parameters, the first observation is a clear change in both CS and QS for Fe^{2+} in Fp, between 51 and 77 GPa. This transition can be associated to a spin transition from high-spin to low-spin state [8]. Such transition pressure is compatible with a Fp phase with a FeO-content ($X_{FeO}/(X_{FeO}+X_{MgO})$) between 0.2 and 0.5 [11]. Based on the analysis of the intensity of the different Mossbauer components present in our samples synthesized at ~77 GPa, we estimate the FeO-content in Fp at 25-30% (see below). At this point, it is worth highlighting that while we observe a brutal

spin change for samples quenched at 300 K for pressures between 41 and 77 GPa, the Fe^{2+}-spin transition in Fp is expected to be progressive in a large pressure range, from ~40 to ~90 GPa, at high temperature [12]. All other CS and QS parameters follow a smooth evolution with pressure compatible with previous works [8,9]. In particular, SMS patterns are well fitted by two different Fe^{2+} contributions in Bg, corresponding to high-spin and intermediate spin, with a significant amount of IS Fe^{2+} above ~30 GPa.

At ~50 GPa, 70% of the Fe is located in Bg (X_{Fe}^{Bg}) as HS-Fe^{2+}, IS-Fe^{2+} and HS-Fe^{3+}, and 30% is located in Fp (X_{Fe}^{Fp}) as HS-Fe^{2+} (Fig. 2b). On the other hand, based on the composition of the starting material, proportions of Bg and Fp in the probed sample are expected to be X_{Bg}=75.3% and X_{Fp}=17.0%. This corresponds to a partitioning coefficient K_D ($X_{Fe}^{Bg}.X_{Mg}^{Fp}/X_{Mg}^{Bg}.X_{Fe}^{Fp}$) of 0.5 to 0.6 (Fig. 3). This value is well compatible with a pioneer study on the role of Al on K_D [13]. We observe a rapid decrease of K_D with increasing pressure up to ~80 GPa (Fig. 3), an effect mostly controlled by transfer of Fe^{2+} from Bg to Fp in this pressure range. Then, the K_D value stabilizes at ~0.2 up to ~130 GPa. In the pressure field where post-Bg becomes a major component, we calculate values of ~0.39(3) or ~0.22(3) for sample synthesis at ~2500 K or ~3500 K, respectively. The higher K_D value measured at 142 GPa, compared to lower pressures, suggest that Fe is less incompatible in post-Bg, compared to Bg, in agreement with a previous report [3].

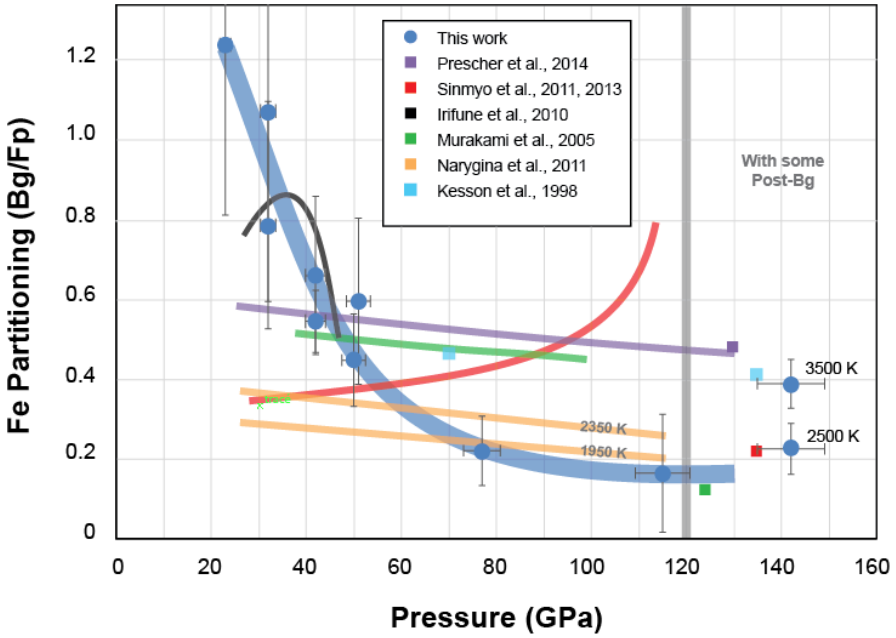

Figure 3: Fe partition coefficient K_D^{Fe} between Bg and Fp. Together with our SMS results, we report previous K_D measurements performed on pyrolite using EELS [1] or EPMA [1-4], or on ringwoodite using in situ XANES measurements [7].

References cited:

1 Prescher, C., Langenhorst, F., Dubrovinsky, L. S., Prakapenka, V. B. & Miyajima, N. The effect of Fe spin crossovers on its partitioning behavior and oxidation state in a pyrolitic Earth's lower mantle system. *Earth Planet. Sci. Lett.* **399**, 86-91, doi:10.1016/j.epsl.2014.05.011 (2014).

2 Sinmyo, R. & Hirose, K. Iron partitioning in pyrolitic lower mantle. *Physics and Chemistry of Minerals* **40**, 107-113, doi:10.1007/s00269-012-0551-7 (2013).

3 Murakami, M., Hirose, K., Sata, N. & Ohishi, Y. Post-perovskite phase transition and mineral chemistry in the pyrolitic lowermost mantle. *Geophys. Res. Lett.* **32**, L03304 (2005).

4 Kesson, S. E., Fitz Gerald, J. D. & Shelley, J. M. Mineralogy and dynamics of a pyrolite lower mantle. *Nature* **393**, 252-255, doi:10.1038/30466 (1998).

5 Andrault, D. *et al.* Experimental evidence for perovskite and post-perovskite coexistence throughout the whole D'' region. *Earth Planet. Sci. Lett.* **293**, 90-96 (2010).

6 Catalli, K., Shim, S. H. & Prakapenka, V. B. Thickness and Clapeyron slope of the post-perovskite boundary. *Nature* **462**, 782-785 (2009).

7 Narygina, O. *et al.* Chemically homogeneous spin transition zone in Earth's lower mantle. *Phys. Earth Planet. Inter.* **185**, 107-111, doi:10.1016/j.pepi.2011.02.004 (2011).

8 Kantor, I. *et al.* Short-range order and Fe clustering in Mg1-xFexO under high pressure. *Phys. Rev. B* **80** (2009).

9 Kupenko, I. *et al.* Electronic spin state of Fe,Al-containing MgSiO3 perovskite at lower mantle conditions. *Lithos* **189**, 167-172, doi:10.1016/j.lithos.2013.10.022 (2014).

10 McCammon, C. *et al.* Stable intermediate-spin ferrous iron in lower-mantle perovskite. *Nat. Geosci.* **1**, 684-687, doi:10.1038/ngeo309 (2008).

11 Fei, Y. W. *et al.* Spin transition and equations of state of (Mg, Fe)O solid solutions. *Geophys. Res. Lett.* **34** (2007).

12 Lin, J. F. *et al.* Spin transition zone in Earth's lower mantle. *Science* **317**, 1740-1743, doi:10.1126/science.1144997 (2007).

13 Wood, B. J. & Rubie, D. C. The effect of alumina on phase transformations at the 660-kilometer discontinuity from Fe-Mg partitioning experiments. *Science* **273**, 1522-1524 (1996).